The Isolated Photon Cross Section in the Central and Forward Rapidity Regions in $p\overline{p}$ Collisions at $\sqrt{s} = 1.8$ TeV

S. Abachi,[14] B. Abbott,[28] M. Abolins,[25] B.S. Acharya,[44] I. Adam,[12] D.L. Adams,[37] M. Adams,[17] S. Ahn,[14] H. Aihara,[22] J. Alitti,[40] G. Álvarez,[18] G.A. Alves,[10] E. Amidi,[29] N. Amos,[24] E.W. Anderson,[19] S.H. Aronson,[4] R. Astur,[42] R.E. Avery,[31] M.M. Baarmand,[42] A. Baden,[23] V. Balamurali,[32] J. Balderston,[16] B. Baldin,[14] S. Banerjee,[44] J. Bantly,[5] J.F. Bartlett,[14] K. Bazizi,[39] J. Bendich,[22] S.B. Beri,[34] I. Bertram,[37] V.A. Bezzubov,[35] P.C. Bhat,[14] V. Bhatnagar,[34] M. Bhattacharjee,[13] A. Bischoff,[9] N. Biswas,[32] G. Blazey,[14] S. Blessing,[15] P. Bloom,[7] A. Boehnlein,[14] N.I. Bojko,[35] F. Borcherding,[14] J. Borders,[39] C. Boswell,[9] A. Brandt,[14] R. Brock,[25] A. Bross,[14] D. Buchholz,[31] V.S. Burtovoi,[35] J.M. Butler,[3] W. Carvalho,[10] D. Casey,[39] H. Castilla-Valdez,[11] D. Chakraborty,[42] S.-M. Chang,[29] S.V. Chekulaev,[35] L.-P. Chen,[22] W. Chen,[42] S. Choi,[41] S. Chopra,[24] B.C. Choudhary,[9] J.H. Christenson,[14] M. Chung,[17] D. Claes,[42] A.R. Clark,[22] W.G. Cobau,[23] J. Cochran,[9] W.E. Cooper,[14] C. Cretsinger,[39] D. Cullen-Vidal,[5] M.A.C. Cummings,[16] D. Cutts,[5] O.I. Dahl,[22] K. De,[45] M. Demarteau,[14] N. Denisenko,[14] D. Denisov,[14] S.P. Denisov,[35] H.T. Diehl,[14] M. Diesburg,[14] G. Di Loreto,[25] R. Dixon,[14] P. Draper,[45] J. Drinkard,[8] Y. Ducros,[40] S.R. Dugad,[44] D. Edmunds,[25] J. Ellison,[9] V.D. Elvira,[42] R. Engelmann,[42] S. Eno,[23] G. Eppley,[37] P. Ermolov,[26] O.V. Eroshin,[35] V.N. Evdokimov,[35] S. Fahey,[25] T. Fahland,[5] M. Fatyga,[4] M.K. Fatyga,[39] J. Featherly,[4] S. Feher,[42] D. Fein,[2] T. Ferbel,[39] G. Finocchiaro,[42] H.E. Fisk,[14] Y. Fisyak,[7] E. Flattum,[25] G.E. Forden,[2] M. Fortner,[30] K.C. Frame,[25] P. Franzini,[12] S. Fuess,[14] E. Gallas,[45] A.N. Galyaev,[35] T.L. Geld,[25] R.J. Genik II,[25] K. Genser,[14] C.E. Gerber,[14] B. Gibbard,[4] V. Glebov,[39] S. Glenn,[7] J.F. Glicenstein,[40] B. Gobbi,[31] M. Goforth,[15] A. Goldschmidt,[22] B. Gómez,[1] G. Gomez,[23] P.I. Goncharov,[35] J.L. González Solís,[11] H. Gordon,[4] L.T. Goss,[46] N. Graf,[4] P.D. Grannis,[42] D.R. Green,[14] J. Green,[30] H. Greenlee,[14] G. Griffin,[8] N. Grossman,[14] P. Grudberg,[22] S. Grünendahl,[39] W.X. Gu,[14,*] G. Guglielmo,[33] J.A. Guida,[2] J.M. Guida,[5] W. Guryn,[4] S.N. Gurzhiev,[35] P. Gutierrez,[33] Y.E. Gutnikov,[35] N.J. Hadley,[23] H. Haggerty,[14] S. Hagopian,[15] V. Hagopian,[15] K.S. Hahn,[39] R.E. Hall,[8] S. Hansen,[14] R. Hatcher,[25] J.M. Hauptman,[19] D. Hedin,[30] A.P. Heinson,[9] U. Heintz,[14] R. Hernández-Montoya,[11] T. Heuring,[15] R. Hirosky,[15] J.D. Hobbs,[14] B. Hoeneisen,[1,†] J.S. Hoftun,[5] F. Hsieh,[24] Tao Hu,[14,*] Ting Hu,[42] Tong Hu,[18] T. Huehn,[9] S. Igarashi,[14] A.S. Ito,[14] E. James,[2] J. Jaques,[32] S.A. Jerger,[25] J.Z.-Y. Jiang,[42] T. Joffe-Minor,[31] H. Johari,[29] K. Johns,[2] M. Johnson,[14] H. Johnstad,[43] A. Jonckheere,[14] M. Jones,[16] H. Jöstlein,[14] S.Y. Jun,[31] C.K. Jung,[42] S. Kahn,[4] G. Kalbfleisch,[33] J.S. Kang,[20] R. Kehoe,[32] M.L. Kelly,[32] L. Kerth,[22] C.L. Kim,[20] S.K. Kim,[41] A. Klatchko,[15] B. Klima,[14] B.I. Klochkov,[35] C. Klopfenstein,[7] V.I. Klyukhin,[35] V.I. Kochetkov,[35] J.M. Kohli,[34] D. Koltick,[36] A.V. Kostritskiy,[35] J. Kotcher,[4] J. Kourlas,[28] A.V. Kozelov,[35] E.A. Kozlovski,[35] M.R. Krishnaswamy,[44] S. Krzywdzinski,[14] S. Kunori,[23] S. Lami,[42] G. Landsberg,[14] J-F. Lebrat,[40] A. Leflat,[26] H. Li,[42] J. Li,[45] Y.K. Li,[31] Q.Z. Li-Demarteau,[14] J.G.R. Lima,[38] D. Lincoln,[24] S.L. Linn,[15] J. Linnemann,[25] R. Lipton,[14] Y.C. Liu,[31] F. Lobkowicz,[39] S.C. Loken,[22] S. Lökös,[42] L. Lueking,[14] A.L. Lyon,[23] A.K.A. Maciel,[10] R.J. Madaras,[22] R. Madden,[15] S. Mani,[7] H.S. Mao,[14,*] S. Margulies,[17] R. Markeloff,[30] L. Markosky,[2] T. Marshall,[18] M.I. Martin,[14] B. May,[31] A.A. Mayorov,[35] R. McCarthy,[42] T. McKibben,[17] J. McKinley,[25] T. McMahon,[33] H.L. Melanson,[14] J.R.T. de Mello Neto,[38] K.W. Merritt,[14] H. Miettinen,[37] A. Mincer,[28] J.M. de Miranda,[10] C.S. Mishra,[14] N. Mokhov,[14] N.K. Mondal,[44] H.E. Montgomery,[14] P. Mooney,[1] H. da Motta,[10] M. Mudan,[28] C. Murphy,[17] F. Nang,[5] M. Narain,[14] V.S. Narasimham,[44] A. Narayanan,[2] H.A. Neal,[24] J.P. Negret,[1] E. Neis,[24] P. Nemethy,[28] D. Nešić,[5] M. Nicola,[10] D. Norman,[46] L. Oesch,[24] V. Oguri,[38] E. Oltman,[22] N. Oshima,[14] D. Owen,[25] P. Padley,[37] M. Pang,[19] A. Para,[14] C.H. Park,[14] Y.M. Park,[21] R. Partridge,[5] N. Parua,[44] M. Paterno,[39] J. Perkins,[45] A. Peryshkin,[14] M. Peters,[16] H. Piekarz,[15] Y. Pischalnikov,[36] V.M. Podstavkov,[35] B.G. Pope,[25] H.B. Prosper,[15] S. Protopopescu,[4] D. Pušeljić,[22] J. Qian,[24] P.Z. Quintas,[14] R. Raja,[14] S. Rajagopalan,[42] O. Ramirez,[17] M.V.S. Rao,[44] P.A. Rapidis,[14] L. Rasmussen,[42] A.L. Read,[14] S. Reucroft,[29] M. Rijssenbeek,[42] T. Rockwell,[25] N.A. Roe,[22] P. Rubinov,[31] R. Ruchti,[32] J. Rutherfoord,[2] A. Santoro,[10] L. Sawyer,[45] R.D. Schamberger,[42] H. Schellman,[31] J. Sculli,[28] E. Shabalina,[26] C. Shaffer,[15] H.C. Shankar,[44] R.K. Shivpuri,[13] M. Shupe,[2] J.B. Singh,[34] V. Sirotenko,[30] W. Smart,[14] A. Smith,[2] R.P. Smith,[14] R. Snihur,[31] G.R. Snow,[27] J. Snow,[33] S. Snyder,[4] J. Solomon,[17] P.M. Sood,[34] M. Sosebee,[45] M. Souza,[10] A.L. Spadafora,[22] R.W. Stephens,[45] M.L. Stevenson,[22] D. Stewart,[24] D.A. Stoianova,[35] D. Stoker,[8] K. Streets,[28] M. Strovink,[22] A. Sznajder,[10] P. Tamburello,[23] J. Tarazi,[8] M. Tartaglia,[14] T.L. Taylor,[31] J. Thompson,[23] T.G. Trippe,[22] P.M. Tuts,[12] N. Varelas,[25] E.W. Varnes,[22] P.R.G. Virador,[22] D. Vititoe,[2] A.A. Volkov,[35] A.P. Vorobiev,[35] H.D. Wahl,[15] G. Wang,[15] J. Warchol,[32] G. Watts,[5] M. Wayne,[32] H. Weerts,[25] F. Wen,[15] A. White,[45] J.T. White,[46] J.A. Wightman,[19] J. Wilcox,[29] S. Willis,[30] S.J. Wimpenny,[9] J.V.D. Wirjawan,[46] J. Womersley,[14] E. Won,[39] D.R. Wood,[29] H. Xu,[5] R. Yamada,[14] P. Yamin,[4] C. Yanagisawa,[42] J. Yang,[28] T. Yasuda,[29] P. Yepes,[37] C. Yoshikawa,[16] S. Youssef,[15] J. Yu,[14] Y. Yu,[41] Q. Zhu,[28] Z.H. Zhu,[39] D. Zieminska,[18] A. Zieminski,[18] E.G. Zverev,[26] and A. Zylberstejn[40]

(DØ Collaboration)

[1] *Universidad de los Andes, Bogotá, Colombia*
[2] *University of Arizona, Tucson, Arizona 85721*
[3] *Boston University, Boston, Massachusetts 02215*
[4] *Brookhaven National Laboratory, Upton, New York 11973*
[5] *Brown University, Providence, Rhode Island 02912*
[6] *Universidad de Buenos Aires, Buenos Aires, Argentina*
[7] *University of California, Davis, California 95616*
[8] *University of California, Irvine, California 92717*
[9] *University of California, Riverside, California 92521*
[10] *LAFEX, Centro Brasileiro de Pesquisas Físicas, Rio de Janeiro, Brazil*
[11] *CINVESTAV, Mexico City, Mexico*
[12] *Columbia University, New York, New York 10027*
[13] *Delhi University, Delhi, India 110007*
[14] *Fermi National Accelerator Laboratory, Batavia, Illinois 60510*
[15] *Florida State University, Tallahassee, Florida 32306*
[16] *University of Hawaii, Honolulu, Hawaii 96822*
[17] *University of Illinois at Chicago, Chicago, Illinois 60607*
[18] *Indiana University, Bloomington, Indiana 47405*
[19] *Iowa State University, Ames, Iowa 50011*
[20] *Korea University, Seoul, Korea*
[21] *Kyungsung University, Pusan, Korea*
[22] *Lawrence Berkeley National Laboratory and University of California, Berkeley, California 94720*
[23] *University of Maryland, College Park, Maryland 20742*
[24] *University of Michigan, Ann Arbor, Michigan 48109*
[25] *Michigan State University, East Lansing, Michigan 48824*
[26] *Moscow State University, Moscow, Russia*
[27] *University of Nebraska, Lincoln, Nebraska 68588*
[28] *New York University, New York, New York 10003*
[29] *Northeastern University, Boston, Massachusetts 02115*
[30] *Northern Illinois University, DeKalb, Illinois 60115*
[31] *Northwestern University, Evanston, Illinois 60208*
[32] *University of Notre Dame, Notre Dame, Indiana 46556*
[33] *University of Oklahoma, Norman, Oklahoma 73019*
[34] *University of Panjab, Chandigarh 16-00-14, India*
[35] *Institute for High Energy Physics, 142-284 Protvino, Russia*
[36] *Purdue University, West Lafayette, Indiana 47907*
[37] *Rice University, Houston, Texas 77251*
[38] *Universidade Estadual do Rio de Janeiro, Brazil*
[39] *University of Rochester, Rochester, New York 14627*
[40] *CEA, DAPNIA/Service de Physique des Particules, CE-SACLAY, France*
[41] *Seoul National University, Seoul, Korea*
[42] *State University of New York, Stony Brook, New York 11794*
[43] *SSC Laboratory, Dallas, Texas 75237*
[44] *Tata Institute of Fundamental Research, Colaba, Bombay 400005, India*
[45] *University of Texas, Arlington, Texas 76019*
[46] *Texas A&M University, College Station, Texas 77843*

A measurement of the cross section for production of single, isolated photons is reported for transverse energies in the range of 10–125 GeV, for two regions of pseudorapidity, $|\eta| < 0.9$ and $1.6 < |\eta| < 2.5$. The data represent 12.9 pb^{-1} of integrated luminosity accumulated in $\bar{p}p$ collisions at $\sqrt{s} = 1.8\,\text{TeV}$ and recorded with the DØ detector at the Fermilab Tevatron Collider. The background, predominantly from jets which fragment to neutral mesons, is estimated using the longitudinal shower shape in the calorimeter. In both pseudorapidity regions the cross section is found to agree with the next-to-leading order QCD prediction for $30 \lesssim E_T^\gamma \lesssim 80\,\text{GeV}$.

Direct photon production probes the parton-parton interaction without the ambiguities associated with jet identification, fragmentation and energy measurement. In $p\bar{p}$ collisions at $\sqrt{s} = 1.8\,\mathrm{TeV}$, the dominant mode of production for low transverse energy photons is through gluon Compton scattering. The cross section is thus sensitive to the gluon distribution in the proton (and antiproton) at low momentum fractions x. With a photon of transverse energy $E_T^\gamma \geq 10\,\mathrm{GeV}$ and pseudorapidity $\eta \leq 2.5$ ($\eta = -\ln\tan\frac{\theta}{2}$, where θ is the polar angle with respect to the proton beam), gluons with momentum fractions as low as $x \sim 10^{-3}$ contribute to the cross section.

Previous collider experiments, including UA2 [1] and CDF [2], have reported an excess of photons at low $E_T^\gamma (\lesssim 30\,\mathrm{GeV})$ compared with the next-to-leading order (NLO) QCD prediction. This may be explained by additional gluon radiation beyond that included in the NLO calculation [3], or by modified parton distributions and fragmentation contributions [4].

This letter presents the first measurement [5] of the cross section for production of isolated photons in $p\bar{p}$ collisions at $\sqrt{s} = 1.8\,\mathrm{TeV}$ with pseudorapidity $1.6 < |\eta| < 2.5$, and a new measurement [6] of the isolated photon cross section in the central region ($|\eta| < 0.9$).

Photons are identified in the DØ detector [7] using a uranium/liquid argon sampling calorimeter housed in a central and two forward cryostats. The calorimeters cover the region of $|\eta| \lesssim 4$ and have electromagnetic energy resolution $\sigma_E/E = 15\%/\sqrt{E(\mathrm{GeV})} \oplus 0.3\%$. In both central and forward regions the electromagnetic section is segmented into four longitudinal layers (EM1–EM4) of 2, 2, 7, and 10 radiation lengths respectively; the transverse segmentation is into towers of size (in pseudorapidity and azimuthal angle) $\Delta\eta \times \Delta\phi = 0.1 \times 0.1$ (0.05×0.05 at shower maximum in EM3). The central and forward drift chambers in front of the calorimeter allow photons to be distinguished from electrons and photon conversions by ionization measurement.

The data presented here represent $12.9 \pm 0.7\,\mathrm{pb}^{-1}$ of integrated luminosity recorded during 1992–93. The detector used a three-level triggering system. The first level used scintillation counters near the beam pipe to detect an inelastic $p\bar{p}$ interaction. The second level was a hardware trigger which summed the electromagnetic energy in calorimeter towers of size $\Delta\eta \times \Delta\phi = 0.2 \times 0.2$. The data used in this analysis were taken with single tower energy thresholds of 2.5, 7, and 10 GeV; all except the highest threshold were prescaled. The third level was a software trigger in which clusters of calorimeter cells were formed and loose cuts made on shower shape. The cluster energy thresholds used at this level were 6, 14, and 30 GeV respectively.

Photon candidates were selected as follows. Fiducial cuts were applied to select candidate clusters away from the calorimeter edges: the clusters were restricted to the regions $|\eta| < 0.9$ and $1.6 < |\eta| < 2.5$, and in the central region were required to be more than 1.6 cm from the azimuthal calorimeter module boundaries. Events where the vertex was more than 50 cm from its nominal position were discarded. The resulting acceptance is $A = 0.73 \pm 0.01$ (0.86 ± 0.01) in the central (forward) regions.

The remaining clusters were identified as photon candidates. No drift chamber tracks were allowed in a tracking road ($\Delta\theta \times \Delta\phi \approx 0.2 \times 0.2$ radians) between the calorimeter cluster and the primary vertex. The efficiency of this requirement was estimated to be 0.85 ± 0.01 (0.61 ± 0.03) in the central (forward) regions. (The inefficiency is due to photon conversions and overlaps with charged tracks from the underlying event.) The photon candidate shower was required to have a shape consistent with that of a single electromagnetic shower and to have more than 96% of its energy in the electromagnetic section of the calorimeter. The candidates were required to be isolated by a cut on the transverse energy in the annular region between $\mathcal{R} = \sqrt{\Delta\eta^2 + \Delta\phi^2} = 0.2$ and $\mathcal{R} = 0.4$ around the cluster: $E_T^{\mathcal{R}\leq 0.4} - E_T^{\mathcal{R}\leq 0.2} < 2\,\mathrm{GeV}$. Finally, the missing transverse energy of the event was required to be less than 20 GeV to reject electrons from $W \to e\nu$ decays and events with large amounts of calorimeter noise. The efficiency of these last three cuts was estimated as a function of E_T^γ using a detailed Monte Carlo simulation of the detector and verified using $Z \to ee$ events. The value obtained was 0.92 ± 0.03 (0.77 ± 0.06) at $E_T^\gamma = 40\,\mathrm{GeV}$ for central (forward) photons.

The primary experimental challenge in the measurement of the direct photon cross section is the extraction of the prompt photon signal from the copious backgrounds due to π^0 and η mesons produced in jets which subsequently decay to photons. While the bulk of this jet background is rejected by the selection criteria listed above, especially by the requirement that the photon candidates be isolated, substantial contamination remains. This comes predominantly from fluctuations in the jet fragmentation which lead to a single meson carrying most of the jet energy. If the meson has transverse energy above about 10 GeV, the showers from its two decay photons coalesce and mimic a single photon shower in the calorimeter.

The fraction of candidates fulfilling the selection criteria which are genuine direct photons (the purity $\mathcal{P}$) was determined using the energy E_1 deposited in the first layer (EM1) of the calorimeter. Neutral meson decays produce two photons, and so the probability that at least one of them undergoes a conversion to an e^+e^- pair in the calorimeter cryostat and first absorber plate is roughly twice that for a single photon. Meson showers therefore start earlier than photon showers leading to larger E_1. A typical distribution of $\log(E_1/E_{\mathrm{total}})$ is shown in Fig. 1. The distribution is fit as the sum of a

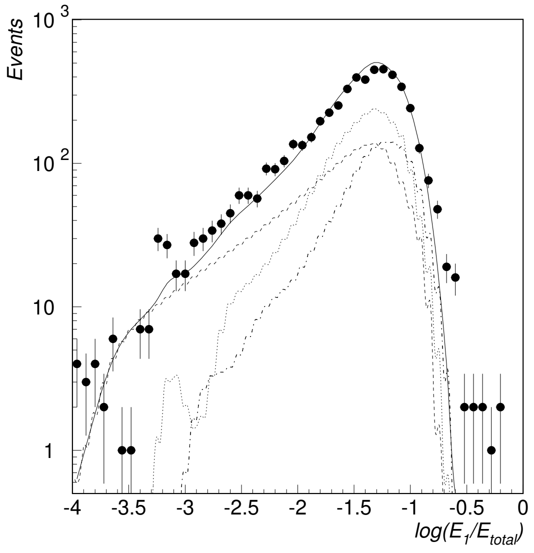

FIG. 1. Distribution of $\log(E_1/E_{\rm total})$ for $E_T^\gamma = 40 \pm 5$ GeV central photon candidates (solid points), and the fitted distribution (solid curve) made up of Monte Carlo photons (dashes), neutral pions (dots), and η mesons (dot-dash curve). The neutral pion and η meson distributions at small $\log(E_1/E_{\rm total})$ fluctuate due to limited Monte Carlo statistics.

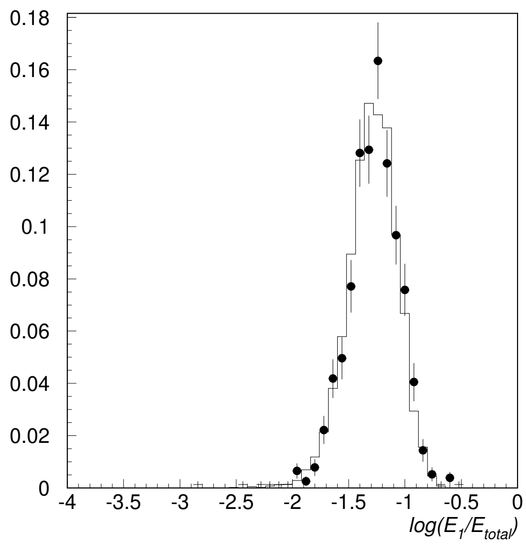

FIG. 2. Normalized distributions of $\log(E_1/E_{\rm total})$ for central electrons from $W \to e\nu$ events (data points), and for single Monte Carlo electrons with $E_T = 40$ GeV (histogram).

photon signal plus π^0 and η meson backgrounds. Fitting was done separately for the central and forward samples for each E_T^γ bin, using χ^2 minimization, and constraining the fractions of signal and background to lie in the range $[0,1]$. The results presented use a production ratio of $\eta/\pi^0 = 1.0$ [8], but all values between 0.50 and 1.25 give essentially indistinguishable results for $\mathcal{P}$ (since the distributions of $\log(E_1/E_{\rm total})$ for π^0 and η mesons are similar). The Monte Carlo calculation combines a detailed simulation of the calorimeter with overlaid minimum bias events from data to model noise, pileup and the underlying event. Its ability to correctly model the $E_1/E_{\rm total}$ distribution has been verified using samples of electrons from $W \to e\nu$ events taken with the same trigger requirements, as shown in Fig. 2.

The combined statistical and systematic error on the purity $\mathcal{P}$, at each E_T^γ point (E_T^γ = 10, 13, 17, 23, 30, 40, 51, and 74 GeV), was estimated by inflating by $\sqrt{\chi^2}$ the error given by the fit to $\log(E_1/E_{\rm total})$ for that E_T^γ. The factor of $\sqrt{\chi^2}$ accounts for systematic differences between the Monte Carlo distributions and the data. It was typically 1.3 in the central region and 1.6 in the forward region. The central and forward photon purities were then corrected by the E_T^γ-dependent efficiencies and fit to the form:

$$\mathcal{P} = 1 - e^{-(a + bE_T^\gamma)}. \tag{1}$$

The data points, fits, and fit errors for $\mathcal{P}$ are shown in Fig. 3.

A second method of purity estimation was used to check the results from the calorimeter energy deposition method. It also takes advantage of the difference in conversion probability between single photons and background. In this case the material between the interaction point and the central or forward drift chamber (CDC or FDC) is considered as a converter and conversions are tagged as tracks with twice minimum ionizing energy using the ionization measurement in the CDC or FDC. The results from the two methods are found to be consistent. The conversion method has larger statistical errors, since only $\sim 10\%$ of photons convert, and therefore it was not used in the fit.

The differential cross section $d^2\sigma/dE_T^\gamma d\eta$ is plotted as a function of E_T^γ in Fig. 4. The next-to-leading order QCD calculation was generated using a program due to Baer, Ohnemus, and Owens [9] which includes γ + jet, γ + dijet and dijet+bremsstrahlung final states. This last is generated from dijet states with collinear bremsstrahlung obtained from a phenomenological photon fragmentation function. In this case, a third collinear jet was created with the remaining jet energy, so that the isolation cut could be modeled including jet energy fluctuations. In all cases the parton energies were smeared using the measured DØ electromagnetic and jet resolutions. The isolation cut is imposed by computing the distance $\mathcal{R}$ in η-ϕ space between the photon and any of the jets, and then rejecting events with a smeared jet $E_T > 2$ GeV within $\mathcal{R} \leq 0.4$ of the photon. (Use of smeared photon and jet energies changes the QCD prediction by less than 4% but better represents the actual measurement.)

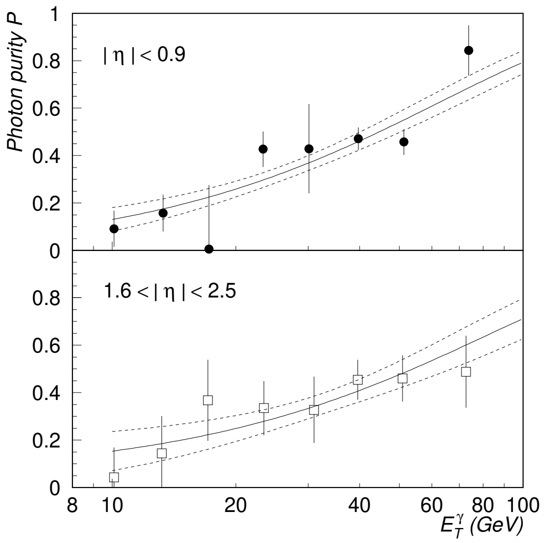

FIG. 3. Efficiency-corrected photon purity ($\mathcal{P}$) vs E_T^γ for central and forward photons. The solid lines show fits of the form $1 - e^{-(a+bE_T)}$ and the dashed lines indicate the range of uncertainty thereon.

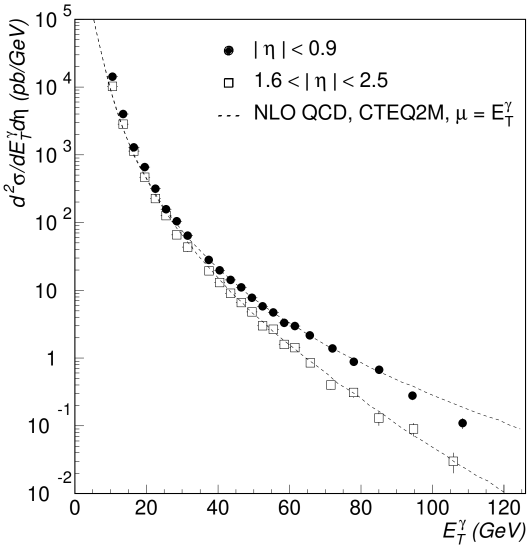

FIG. 4. The inclusive isolated photon cross section $\sigma_e = d^2\sigma/dE_T^\gamma\,d\eta$ as a function of photon transverse energy E_T^γ, for central (circles) and forward regions (squares). The errors are statistical only. The NLO QCD calculated cross sections σ_t, using CTEQ2M parton distributions with $\mu = E_T^\gamma$, are shown for comparison.

The CTEQ2M parton distributions [10] and renormalization scale $\mu = E_T^\gamma$ were used. If instead the CTEQ2MF or CTEQ2MS parton distributions were used, or scales of $\mu = 2E_T^\gamma$ or $E_T^\gamma/2$ were employed, then the predicted cross section changes by $\lesssim 6$ %.

Figure 5 shows a plot of $(\sigma_e - \sigma_t)/\sigma_t$ where σ_e and σ_t are respectively the experimental and theoretical values of the differential cross section $d^2\sigma/dE_T^\gamma\,d\eta$. The shaded band in the figure shows the magnitude of the systematic error, which is estimated by adding in quadrature the uncertainties resulting from the acceptance ($\sim 1\%$), the trigger and selection efficiencies (3–5%), the photon purity (Fig. 3), the luminosity (5%), and the electromagnetic energy scale of the calorimeter (1% in the central, 4% in the forward region). The measured cross sections are in good agreement with the NLO QCD prediction for both central and forward regions for moderate transverse energies, $30 \lesssim E_T^\gamma \lesssim 80$ GeV. The data points for both the central and forward cross sections lie above the NLO QCD prediction at lower transverse energies, but given the magnitude of the systematic error no strong conclusion can be drawn. At the highest transverse energies probed, the data for the central region lie below the QCD prediction. Above $E_T^\gamma = 74$ GeV the photon purity $\mathcal{P}$ is the result of an extrapolation; the increased systematic error at large E_T^γ reflects the resulting uncertainty.

The ratio of forward to central cross sections is shown in Fig. 6. The systematic error on the ratio is estimated by adding those for the two regions in quadrature, with the exception of the luminosity uncertainty which cancels. The ratio is in good agreement with the NLO QCD expectation for large transverse momenta, but the data lie below NLO QCD for $x_T \lesssim 0.04$ ($E_T^\gamma \lesssim 36$ GeV). Given the magnitude of the systematic error, no strong conclusion can be drawn. This ratio of cross sections, which depends on our unique measurement of the forward photon cross section, could be used to constrain the gluon distribution function at low x. However, a complete understanding of the origin of the low-E_T^γ behavior of the photon cross section is needed before information on the gluon distribution can be extracted.

ACKNOWLEDGEMENTS

We thank the Fermilab Accelerator, Computing, and Research Divisions, and the support staffs at the collaborating institutions for their contributions to the success of this work. We also acknowledge the support of the U.S. Department of Energy, the U.S. National Science Foundation, the Commissariat à L'Energie Atomique in France, the Ministry for Atomic Energy and the Ministry of Science and Technology Policy in Russia, CNPq in Brazil, the Departments of Atomic Energy and Science and Education in India, Colciencias in Colombia, CONACyT in Mexico, the Ministry of Education, Research Foundation and KOSEF in Korea, CONICET and UBACYT in Argentina, and the A.P. Sloan Foundation.

* Visitor from IHEP, Beijing, China.

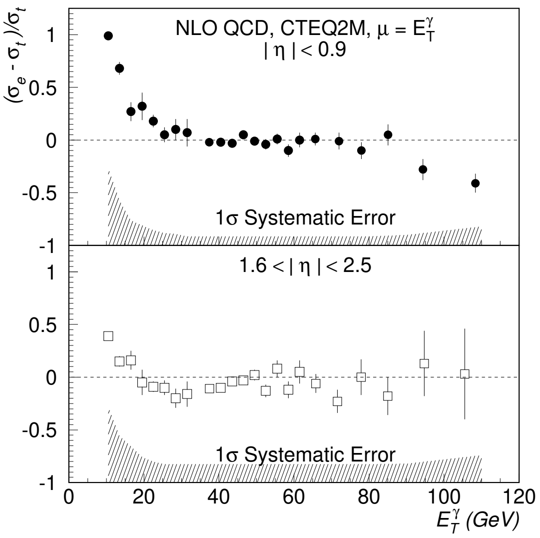

FIG. 5. Difference between the measured isolated photon cross section σ_e and the NLO QCD prediction σ_t, normalized to the latter. The shaded bands show the magnitude of the combined systematic errors ($1\,\sigma$) for each of the two regions.

† Visitor from Univ. San Francisco de Quito, Ecuador.

[1] UA2 Collaboration, J. Alitti *et al.,* Phys. Lett. **B263** (1991) 544.

[2] CDF Collaboration, F. Abe *et al.,* Phys. Rev. Lett. **68** (1992) 2734;
CDF Collaboration, F. Abe *et al.,* Phys. Rev. D **48** (1993) 2998;
CDF Collaboration, F. Abe *et al.,* Phys. Rev. Lett. **73** (1994) 2662.

[3] J. Huston *et al.,* Phys. Rev. D **51** (1995) 6139.

[4] M. Glück, L.E. Gordon, E. Reya, and W. Vogelsang, Phys. Rev. Lett. **73** (1994) 388;
W. Vogelsang and A. Vogt, Nucl. Phys. **B453** (1995) 334;
E. Quack and D.K. Srivastava, "A Global Test of QCD Theories for Direct Photon Production," GSI-94-40, August 1995.

[5] S.T. Fahey, Ph.D. Thesis, Michigan State University, 1995 (unpublished).

[6] Y.-C. Liu, Ph.D. Thesis, Northwestern University, 1996 (unpublished). Accessible via the World Wide Web at **http://d0sgi0.fnal.gov/publications_talks/thesis/thesis.html**.

[7] DØ Collaboration, S. Abachi *et al.*, Nucl. Instrum. Methods **A338** (1994) 185.

[8] CDF Collaboration, F. Abe *et al.,* Phys. Rev. D **48** (1993) 2998.

[9] H. Baer, J. Ohnemus, and J.F. Owens, Phys. Rev. D **42** (1990) 61.

[10] CTEQ Collaboration, J. Botts *et al.*, Phys. Lett. **B304** (1993) 159.

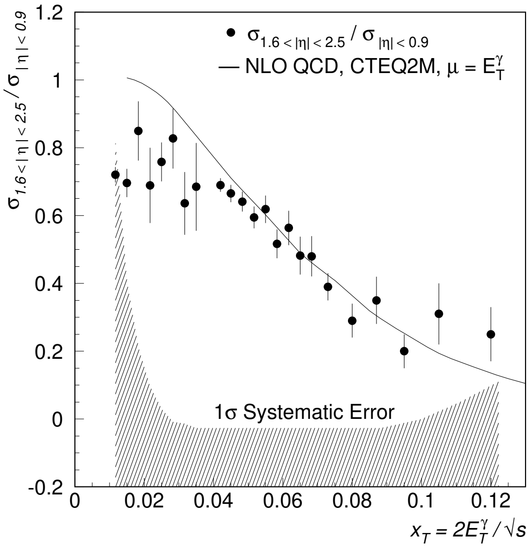

FIG. 6. Ratio of inclusive isolated photon cross sections $d^2\sigma/dx_T\,d\eta$ in the forward region to the central region. The NLO QCD prediction with CTEQ2M parton distributions is shown for comparison. The shaded band shows the magnitude of the combined systematic error.